Mesopelagic fish gas bladder elongation, as estimated from wideband acoustic backscattering measurements

Babak Khodabandeloo, Egil Ona, Geir Pedersen, et al.

ARTICLES YOU MAY BE INTERESTED IN

JASA

Mesopelagic fish gas bladder elongation, as estimated from wideband acoustic backscattering measurements

Babak Khodabandeloo,[1,a] Egil Ona,[1] Geir Pedersen,[1] Rolf Korneliussen,[1] Webjørn Melle,[2] and Thor Klevjer[2]

[1]*Ecosystem acoustics research group, Institute of Marine Research, P.O. Box 1870 Nordnes, 5817 Bergen, Norway*
[2]*Plankton research group, Institute of Marine Research, P.O. Box 1870 Nordnes, 5817 Bergen, Norway*

ABSTRACT:

Backscattered acoustic energy from a target varies with frequency and carries information about its material properties, size, shape, and orientation. Gas-bearing organisms are strong reflectors of acoustic energy at the commonly used frequencies ($\sim$18–450 kHz) in fishery surveys, but lack of knowledge of their acoustic properties creates large uncertainties in mesopelagic biomass estimates. Improved knowledge about the volume and elongation (i.e., longest to shortest dimension) of swimbladders of mesopelagic fishes has been identified as an important factor to reduce the overall uncertainties in acoustic survey estimates of mesopelagic biomass. In this paper, a finite element approach was used to model gas-filled objects, revealing the structure of the backscattering, also at frequencies well above the main resonance frequency. Similar scattering features were observed in measured broadband backscattering of several individual mesopelagic organisms. A method is suggested for estimating the elongation of a gas-bubble using these features. The method is applied to the *in situ* measured wideband (33–380 kHz) target strength (TS) of single mesopelagic gas-bearing organisms from two stations in the North Atlantic (NA) and Norwegian Sea (NS). For the selected targets, the method suggested that the average elongation of gas-bladder at the NA and NS stations are 1.49 ± 0.52 and 2.86 ± 0.50, respectively.

I. INTRODUCTION

Mesopelagic fish, i.e., those fish that for at least part of the day reside at depths between 200 and 1000 m, are an important component of open ocean ecosystems (Marshall, 1951). Many of them perform a diel vertical migration (DVM), and may be major contributors to the biological pump (Klevjer *et al.*, 2016; Vinogradov, 1962). They are also rich in protein and omega-3 oils and have lately received interest as a potential feed for the aquaculture industry (Grimaldo *et al.*, 2020; Olsen *et al.*, 2020) or as a novel future food source (Naik *et al.*, 2021). Major uncertainties in the worldwide biomass estimates of mesopelagic fish (Gjoesaeter and Kawaguchi, 1980) hamper our understanding of the role and importance of mesopelagic fish biomass and also of the functioning of the open ocean ecosystems themselves. Current global biomass estimates range roughly between 1 to 20 Gt (Proud *et al.*, 2019). If the true biomass is in the higher part of this range, it suggests that transfer efficiencies, i.e., the amount of energy transferred between adjacent trophic levels, exceed a commonly applied rule of thumb (10%), suggesting that we have a limited understanding of how energy flows in pelagic food-chains (Irigoien *et al.*, 2014).

Echosounder data are commonly used to map mesopelagic resources, as the habitat is hard to reach with common sampling gear, such as trawls. Acoustic waves propagate efficiently in the water and scatter when reaching objects with different impedance along the way. Part of this acoustic energy is scattered back toward the source and carries information about the object size, shape, orientation, and material properties. State-of-the-art acoustic equipment and techniques have made it possible to transmit and receive acoustic energy to monitor the marine environment at spatial and temporal scales that have been inaccessible previously (Godø *et al.*, 2014). Introduction of broadband echosounders to fishery acoustics has made it possible to obtain backscattering measurement of organisms over a range of frequencies (Andersen *et al.*, 2013; Chu, 2011; Stanton *et al.*, 2003). While it is challenging to convert acoustic backscatter measurements to estimates of biomass, the frequency dependence of scattering also offers opportunities with regard to acoustic identification, as wideband echosounders provide backscattering variation with frequency (Zakharia, 1996; Korneliussen *et al.*, 2016; Bassett *et al.*, 2020; Agersted *et al.*, 2021b).

Gas-filled organs, such as swimbladders, are strong reflectors of incident acoustic energy, and may contribute more than 90%–95% of the mean backscattering from an insonified fish (Foote, 1980). The observed magnitude and spectral characteristics of the backscattering is mainly due to the gas inclusion, and the remainder of the body of the fish has minor effects (Au and Benoit-Bird, 2003; Haslett, 1965; Love, 1971). A global sensitivity analysis indicated

a)Electronic mail: khodabandeloo.babak@gmail.com

that fish swimbladder volume, its elongation (i.e., the ratio of the longest to the shortest dimension), and size distribution in mesopelagic fish are the main sources of uncertainties in the global biomass estimates (Proud *et al.*, 2019). Separation of fish from other gas bearing organisms, e.g., physonect and cystonect siphonophores, are also important, as misinterpretation of backscatter from siphonophores will lead to overestimations of the fish biomass.

A gas-inclusion's morphological features, particularly size and shape (e.g., elongation), have noticeable effects on the backscattering (Love, 1978; Yasuma *et al.*, 2003), especially at frequencies well above the main resonance (Khodabandeloo *et al.*, 2021a). Elongating a gas sphere, while keeping the volume the same, will shift the resonance to higher frequencies (Ye, 1997). Elongated swimbladders are acoustically directional, especially at higher frequencies. Therefore, knowledge of swimbladder morphology is crucial for quantitative analysis of the measured backscattering from the targets possessing it. One approach to obtain morphological measurements of the swimbladder is x-ray imaging (Fujino *et al.*, 2009; Sobradillo *et al.*, 2019; Yasuma *et al.*, 2010). To enhance backscattering estimation of Mueller's pearlside, soft x-ray imaging has been used for morphological measurements of swimbladders (Sobradillo *et al.*, 2019), but direct morphological measurements by necessity require that the organisms be brought up to surface and onboard vessels, and the impacts of capture and handling on these internal structures are unknown (Ona, 1990). Acoustic backscattering measurements can therefore be used to provide non-extractive *in situ* estimates of gas-bladder morphology.

In this paper, we use an acoustic inversion procedure to estimate elongation of mesopelagic gas-inclusions *in situ*, without requiring capture and handling. Subsequently, knowing the elongation helps to estimate the size (i.e., volume) more accurately. To model the backscattering from gas-filled objects, we used finite element method (FEM) instead of simplified methods (Clay and Horne, 1994; Love, 1978; Ye, 1997) which fail to provide accurate results especially for higher frequency regions where the wavelength is small compared to the object size. Many of these methods provide a backscattering estimation at the cost of losing accuracy and generality of the solution through various approximations and simplifications such as truncation of higher order backscattering modes. Using FEM, we are able to model all the resonances which appear as peaks and nulls in the backscattering [or target strength (TS) in logarithmic scale] frequency response. The modeling results were compared to the measured TS frequency response of several individual mesopelagic organisms, which were collected by deploying broadband echosounders within the mesopelagic layer.

II. METHOD

A. Finite element method (FEM) for backscattering modeling

FEM is a robust technique to solve differential equations over a certain region or domain. FEM divides the physical domain into subdomains, so-called finite elements, within which an approximate or exact solution can be obtained. The approximation of the solution over each element is expressed as an interpolation function over the element assuming the variable is known at certain points, so-called nodal points, in the element. The nodal points often lie on the element boundaries where two adjacent elements are interconnected. The element equations in the matrix form are derived by substituting the approximate solution into the weak formulation, which is the differential equation in the integral form. Utilizing the connectivity of elements, the element matrices are assembled into a global matrix to obtain the equations for the entire domain. The solution is found by satisfying the prescribed boundary conditions on the dependent variables or their derivatives (Ottosen and Petersson, 1992; Rao, 2011).

To estimate the scattered wave from an object with boundaries Γ within an exterior domain Ω bounded by an artificial exterior boundary Γ_{art}, we utilize a time-harmonic acoustic model governed by the Helmholtz equation

$$\nabla^2 p + k^2 p = -q \quad \text{in} \quad \Omega, \tag{1}$$

where ∇^2 is the Laplace operator, p is the total acoustic pressure, k is the wave number, and q is the external force.

Helmholtz equation (1) is used in conjunction with boundary conditions (2)–(4) [see Harari (2006), Ihlenburg (1998), Kechroud *et al.* (2004), and Thompson (2006)],

$$p = g \quad \text{on} \quad \Gamma_g, \tag{2}$$

$$\partial p / \partial n = ikh \quad \text{on} \quad \Gamma_h, \tag{3}$$

$$\partial p / \partial n = -Mp \quad \text{on} \quad \Gamma_{art}. \tag{4}$$

In the above equations, $i = \sqrt{-1}$ is the imaginary unit, g and h are prescribed boundary conditions, and M is a linear operator called Dirichlet to Neumann (DtN) which imposes a relation between the unknown function and its normal derivative, on Γ_{art}. The unit vector normal to the boundaries is shown by n. It is assumed that partitioning of the object boundary satisfies $\Gamma_g \cup \Gamma_h = \Gamma$ and $\Gamma_g \cap \Gamma_h = \emptyset$.

The artificial exterior boundary, Γ_{art}, is introduced to truncate the unbounded exterior domain and form a bounded computational domain which can be handled by FEM. In other words, the infinite domain is replaced by the artificial exterior boundary and guarantees the nonreflecting condition at Γ_{art}.

The boundary value problem is solved by the finite element method (FEM) implemented in COMSOL MULTIPHYSICS® version 5.6. The artificial exterior boundary is modeled by perfectly matched layer (PML) formulation (Berenger, 1994). The objective is to have a layer of finite thickness around the bounded computational domain to absorb the outgoing waves within this layer and effectively reduce their reflection (Harari, 2006; Thompson, 2006). At least 18 elements per wavelength were used to discretize the target and the surrounding water domains.

4074   J. Acoust. Soc. Am. **151** (6), June 2022

Khodabandeloo *et al.*

The swimbladder was modeled as a gas-filled prolate spheroid. It was assumed that the swimbladder of physoclist mesopelagic fish is mainly filled with oxygen (Berg and Steen, 1968; Ross, 1976; Wittenberg *et al.*, 1980). In all cases the speed of sound inside the gas-bladder is assumed $325 \, \text{m s}^{-1}$. The sound speed and density of surrounding water are assumed $1500 \, \text{m s}^{-1}$ and $1027 \, \text{kg m}^{-3}$, respectively. In addition, the effects of deviation from the prolate spheroid shape were investigated by modeling the swimbladder as ellipsoid and egg-shaped gas-filled objects. Both prolate spheroids and egg-shapes are axisymmetric, but the egg-shape is thicker at one end. The backscattering from an ellipsoid was estimated by a three-dimensional model (Khodabandeloo *et al.*, 2021b). On the other hand, to reduce the computational cost, a two-dimensional axisymmetric model was used for prolate spheroids or other axisymmetric objects (Khodabandeloo *et al.*, 2021a) (see Fig. 1). The latter approach is especially useful for backscattering estimation at higher frequencies. However, even though the scattering object is axisymmetric, the planar incident wave is not. One way to include the planar wave in the axisymmetric model, is to expand the planar incident wave (e.g., propagating in x-direction) into a series of cylindrical waves (r, θ, and z coordinates) by Jacobi–Anger expansion (Cakoni and Colton, 2005), as

$$e^{ikx} = e^{ikr\cos\theta} = \sum_{m=-\infty}^{+\infty} i^m J_m(kr) e^{im\theta}, \qquad (5)$$

where J_m is an m*th* Bessel function of the first kind.

Far-field backscattered pressure is required to calculate TS. Extending the computational domain and solving the
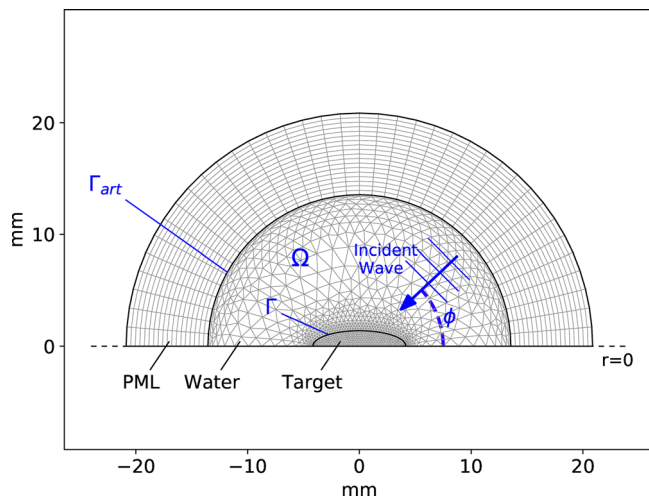

FIG. 1. (Color online) A 2D axisymmetric FEM model for a prolate spheroid with the elongation $\alpha = 3$. The domain is for the 50 kHz backscattering estimation. For lower frequencies, the water domain size is increased to ensure at least 18 elements per wavelength. While for higher frequencies, the water domain is decreased to ensure 18 elements per wavelength and avoid unnecessarily large number of elements. Water domain is surrounded by perfectly matched layer (PML). By revolving ($\theta : 0 \rightarrow 2\pi$) the profiles around the axis of symmetry (z-axis in cylindrical coordinate shown by $r = 0$), the three-dimensional objects are formed. ϕ is the planar wave incident angle.

Helmholtz equation to estimate the pressure at a large distance is not practical. For a homogeneous medium, solution at any point outside a closed surface that encompasses all sources and scatterers can be calculated by Helmholtz-Kirchhoff integral provided that both Dirichlet and Neumann values are known on the surface. The far-field backscattered pressure, p_{far}, was calculated using the appropriate Green's function at a sufficiently large distance ($D \rightarrow \infty$) where the oscillating phase factor can be ignored (COMSOL Multiphysics, 2020),

$$p_{far}(\boldsymbol{D}) = -\frac{1}{4\pi} \int_S e^{ik\frac{r\cdot D}{|D|}} \left(\nabla p(r) - ikp \frac{\boldsymbol{D}}{|\boldsymbol{D}|} \right) \cdot \boldsymbol{n} dS, \qquad (6)$$

where S is a closed surface surrounding the target and **n** is a normal unit vector into the domain enclosed by the surface S. Reliable estimation of the pressure in the exterior field by Kirchhoff–Helmholtz integral (6) requires accurate numerical estimate of the normal derivative of pressure on S. To achieve this, a thin (thickness $= \lambda_w/200$) single boundary layer mesh element is added on the inside of water domain adjacent to PML layer. $\lambda_w = 2\pi f / c_w$ is the wavelength in the water domain where f and c_w are the frequency and water sound speed, respectively.

TS is calculated as (MacLennan, 1981; Reeder *et al.*, 2004)

$$\text{TS} = 20\log_{10}\left(\left| D p_{far}(\boldsymbol{D}) \right| / |p_{inc}| \right). \qquad (7)$$

B. Acoustic data collection

The acoustic data presented in this paper were collected during a research cruise on board RV "G.O. Sars" [Institute of Marine Research (IMR), Norway] in the North Atlantic (NA) and the Norwegian Sea (NS) in June 2021. The *in situ* wideband TS frequency response of single gas-bearing mesopelagic targets (e.g., swimbladdered mesopelagic fish) were measured using a submersible platform (MESSOR) (Knutsen *et al.*, 2013) equipped with broadband echosounders (Simrad EK80 WBT tubes connected to transducers with nominal frequencies of 38, 70, 120, 200, and 333 kHz). The echosounders were operated with simultaneous pinging with 3–4 pings per second and an observation range of 75 m. The cross-channel interference (crosstalk) was reduced by adjusting the power settings (Khodabandeloo *et al.*, 2021c). The settings for operating the echosounders are given in Table I. Because of 2.048 ms pulse duration, the frequency resolution of collected wideband TS was approximately 0.5 kHz. In total 83 single targets were manually selected, where 43 targets were from NA, station 171 (61.90°N, –24.70°E) and 40 targets from NS, station 178 (63.63°N, 4.13°E). To ensure that each selected target represents a single organisms and the echoes from adjacent targets are not included, the frequency response of each ping and the target locations within the beam were carefully monitored [see Khodabandeloo *et al.* (2021b)]. The echosounders were calibrated according to Simrad procedures for narrowband

J. Acoust. Soc. Am. **151** (6), June 2022

Khodabandeloo *et al.*   4075

TABLE I. EK80 settings for data collection.

Parameters	38 kHz	70 kHz	120 kHz	200 kHz	333 kHz
Transducer	ES38-18DK	ES70-7CD	ES120-7CD	ES200-7CD	ES333-7CD
Frequency [kHz]	35–45	50–88	90–158	160–258	280–380
Pulse duration [ms]	2.048	2.048	2.048	2.048	2.048
Transmit power [W]	90	50	80	135	50
Equivalent beam angle [dB]	−12.5	−20.7	−20.7	−20.7	−20.7

continuous wave (CW) and broadband frequency modulated (FM) calibrations (Simrad, 2020).

III. RESULTS

A. Effects of elongation, angle of incidence, and depth on backscattering of prolate spheroids

The TS frequency response of a target depends on its morphology and material properties. In this work, we study how the elongation factor (i.e., aspect ratio), incident angle, and depth (which affects the density of gas inside swimbladder) affect the TS frequency response.

Our main focus is on the location of the first and second resonant peaks of modeled TS of a prolate spheroid (Fig. 2).

It is observed that when increasing the elongation (α = major to minor axis), there is a slight shift of the first peak to higher frequencies but also a considerable shift of the second peak towards lower frequencies [Fig. 2(b)]. The incidence angle does not change the location of peaks. However, by increasing the incident angle, the amplitude of the second resonance decreases and the second resonance peak vanishes for the broadside incidence ($\phi = 90°$) [Fig. 2(c)]. Since echosounder beams often are vertically oriented, varying incident angle on targets is similar to tilt-angle (orientation) of the swimbladder. To better observe the overlapping curves in Fig. 2(c), they are also plotted separately (see Fig. 10). An increase in depth while keeping the gas-bladder volume unchanged, which corresponds to an
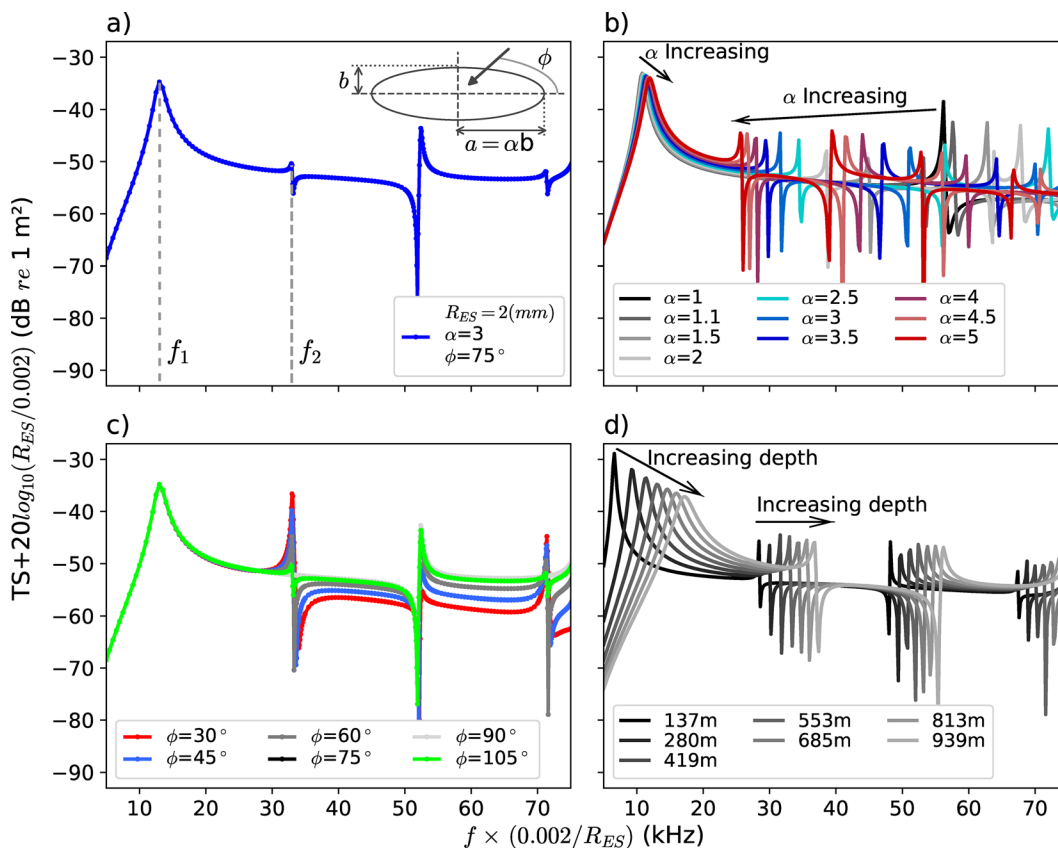

FIG. 2. (Color online) (a) TS frequency response of a prolate spheroid with equivalent spherical radius (R_{ES}) of 2 mm and the elongation of 3 for the incident angle of 75°. First and second resonant peak frequencies are denoted f_1 and f_2, respectively. (b) Effects of increasing elongation from $\alpha = 1$ to $a = 5$ on the first and second peak frequencies of a prolate spheroid with R_{ES}=2 mm equivalent spherical radius and $\phi = 60°$. (c) TS frequency response of a prolate spheroid (R_{ES}=2 mm, $\alpha = 3$) for four different incident angles $\phi = 45°$, 60°, 75°, 90°, and 105°. The second peak is absent for the broadside incidence. (d) Effects of increasing depth from 137 m to 939 m on the first and second peak frequencies for a prolate with $R_{ES} = 2$ mm $\phi = 60°$. The frequency resolution of modeled TS for subplots "a" and "c" is 0.1 kHz around the higher frequency resonance peaks and 0.5 kHz elsewhere. For subplots "b" and "d," the frequency resolution is 0.2 kHz.

4076   J. Acoust. Soc. Am. **151** (6), June 2022
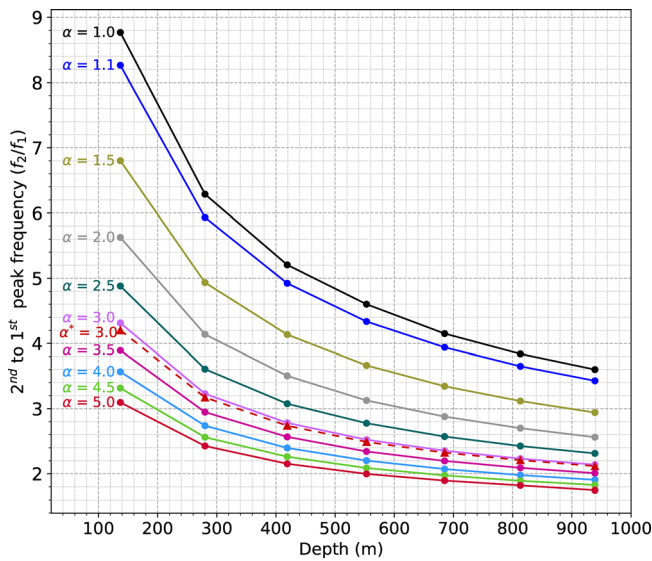
Khodabandeloo et al.

FIG. 3. (Color online) Ratio of 2nd to 1st peak resonance frequency for different elongations at different depths for an oxygen filled prolate spheroid. Solid line are derived from the prolate spheroid model. Dashed line with triangular points indicates the egg shaped swimbladder (asterisk α) (see Fig. 4). To generate this plot, the first and second resonance peak frequencies were detected from the TS frequency responses for the incident angle of 60°. However, other incident angles (except 90° where the second resonance peak is absent) will produce the same result, as the location of the resonance peak frequencies are independent of incident angle [see Fig. 2(c) and Fig. 10].

increase in the gas density within the swimbladder, shifts the resonances to higher frequencies [Fig. 2(d) and Fig. 13 in the Appendix]. Since many mesopelagic fish have a closed (physoclistous) swimbladder that is used to maintain a neutral bouyancy (Marshall, 1960), the assumption of constant volume is valid for them.

B. Elongation estimation of gas-bladder by the location of the first and second resonance peaks

Members of the dominant taxa of mesopelagic fish (e.g., Myctophids and Gonostomatids) are physoclistous [e.g., with a closed swimbladder (Marshall, 1960)]. For a

given fish, the volume of the swimbladder is therefore likely independent of depth, since most observations of mesopelagic fish suggest neutral buoyancy, and the swimbladder is the main mechanism for achieving this (Barham, 1963; Kaartvedt *et al.*, 2009; Marshall, 1960). However, since changing the size while maintaining the shape will scale the frequency axis, using the ratio of the frequencies of the peaks will make the results independent of the size of the swimbladder (for more details see the Appendix). The ratio of second to the first resonance peak frequency (f_2/f_1) for different elongations is plotted as a function of depth (Fig. 3). Having the first and second resonance frequencies of a gas-bearing target at a known depth, it is possible to estimate the elongation of its gas sac based on Fig. 3. For example, a target located at a depth of 700 m, with a $f_2/f_1 = 3.3$, should have an elongation of 1.5. The effects of deviation from a prolate spheroid on f_2/f_1, which are studied in Sec. III C, is included in Fig. 3 and shown by a dashed line. For the studied example, the deviation from a prolate spheroid does not significantly affect the elongation estimation.

C. Impact of deviation from prolate spheroid on the location of resonance frequencies

A gas-bladder usually has a complex morphology and some simplifications are inevitable to study it systematically. Here, we have used a prolate spheroid to study the elongation effects of a gas-bladder on its backscattering, specifically the first and second peak frequencies of the TS frequency response. A prolate spheroid is formed by rotating an ellipse about its major axis (Fig. 4) and therefore is an axisymmetric object. To evaluate whether the prolate spheroid is a representative model to study the elongation of a generic gas-bladder, the effects of deviation from a prolate spheroid on the resonance frequencies are studied by two cases. (1) An egg-shape which is created from rotation of an asymmetric tapered oval shape (i.e., one end bigger than the other) about its symmetry axis (r = 0) (Fig. 4). (2) An ellipsoid, which unlike the prolate spheroid, does not have equal semi-minor axes ($b \neq c$ in Fig. 5) and therefore is non-axisymmetric. In all cases the volume of the objects and the
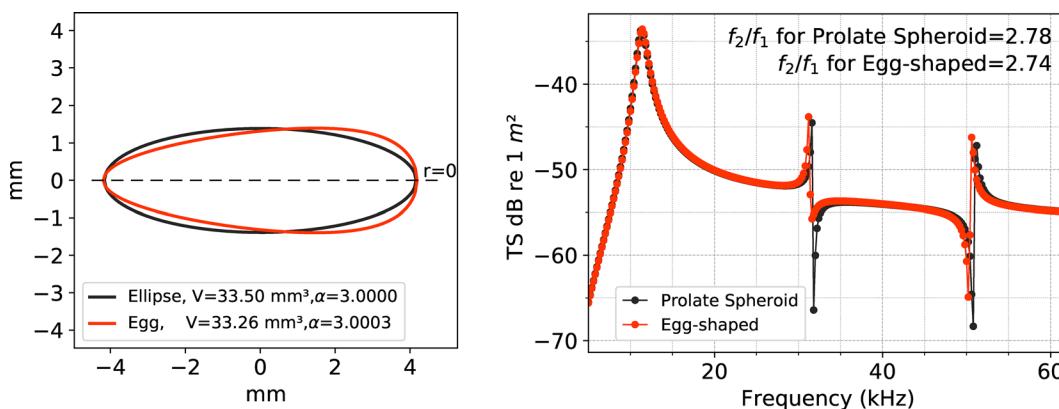

FIG. 4. (Color online) Left panel: Profile of a prolate spheroid and egg shape. The rotation axis (r = 0) is shown by dashed line. Right panel: Modeled TS for the prolate spheroid and egg-shaped objects for incident angle of $\phi = 60°$. First (f_1) and second (f_2) peak frequencies of a gas filled prolate spheroid and egg shape object with almost the same volumes and elongations were detected and f_2/f_1 was obtained for each object.
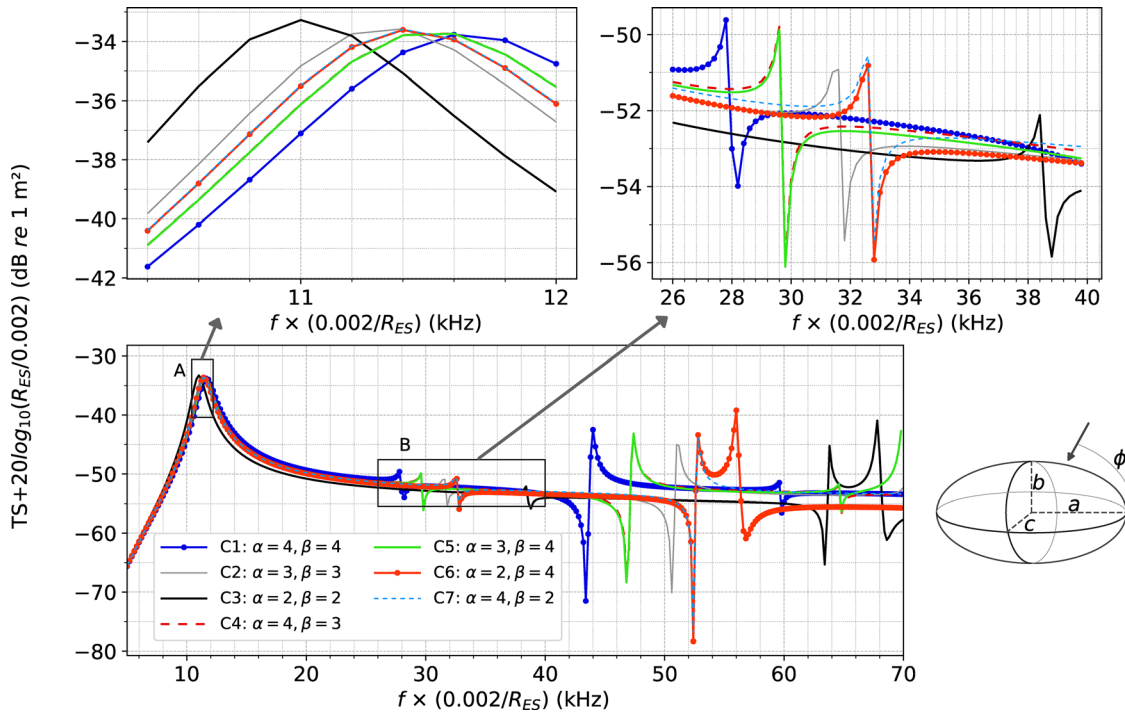
J. Acoust. Soc. Am. **151** (6), June 2022

Khodabandeloo *et al.*   4077

FIG. 5. (Color online) Target strength frequency response of ellipsoid with $R_{ES} = 2$ mm, the gas density of 60 kg m^{-3} for different $\alpha = a/b$ and $\beta = a/c$ where "a" is semi-major axis, "b" and "c" are the semi-minor axes. The TS frequency responses are modeled for $75°$ incident angle. The incident wave is normal to the semi-minor axis shown by "c."

sound speeds and densities of gas and surrounding water were kept the same. For the first case (Fig. 4), the volumes generated by the shown profiles have around 0.7% difference, while their elongations are almost the same ($\sim 0.01\%$ difference). The modeled backscattering results for the two objects show a $\sim 1.4\%$ difference in the ratios of 2nd to 1st peak frequencies (Fig. 4).

In the second case, the backscattering from ellipsoids of same volume ($R_{ES} = 2$ mm) but different shapes (i.e., different $\alpha = b/a$ and $\beta = c/a$), where "b" and "c" are the semi-minor axes while "a" is semi-major axis of the ellipsoid, are estimated (Fig. 5). Three of them (C1-3) are backscattering from prolate spheroids (i.e., $\alpha = \beta$). The first and second peak frequencies are identified in each of the TS frequency responses and the ratio of f_2/f_1 are summarized in Table II. It is observed that swapping "b" and "c" (e.g., C4-5 or C6-7) does not affect the location of f_1 and f_2 and therefore

TABLE II. The ratio f_2/f_1 obtained from modeled TS frequency responses of different ellipsoids but with the same volume. The gas density used for the modeling was 60 kg m^{-3}.

			f_2/f_1
C1	Prolate spheroid	$\alpha = 4, \beta = 4$	2.38
C2	Prolate spheroid	$\alpha = 3, \beta = 3$	2.78
C3	Prolate spheroid	$\alpha = 2, \beta = 2$	3.48
C4	Ellipsoid	$\alpha = 4, \beta = 3$	2.57
C5	Ellipsoid	$\alpha = 3, \beta = 4$	2.57
C6	Ellipsoid	$\alpha = 2, \beta = 4$	2.85
C7	Ellipsoid	$\alpha = 4, \beta = 2$	2.85

they have the same f_2/f_1. The other observation is that C1 has the same α and β as α of C7 and β of C6, however, its f_2/f_1 is $\sim 16\%$ smaller than that of C6 and C7. Similarly, C3 has the same α and β as α of C6 and β of C7, but its f_2/f_1 is $\sim 22\%$ larger than that of C6 and C7. On the other hand, the ratio f_2/f_1 of C2 has $\sim 2\%$ difference compared to that of C6 or C7. Note that α and β of C2 are equal to $(\alpha + \beta)/2$ of C6 or C7.

D. *In situ* measurements of TS(f)

From the wideband data collected by MESSOR at two different stations 171 (NA) and 178 (NS), TS frequency responses of several single targets derived from pulse compressed signals were selected, and the results are presented here. TS of individual registrations (pings) for three single targets and their location in the echosounder beams are shown in Fig. 6. The athwartships offsets of the target locations (horizontal axis in Fig. 6) are due to horizontal offsets between the transducers and/or due to the acoustical axis of all transducers not being parallel. The TS locations of the target estimated by 38 kHz do not always correspond well with the other frequencies, especially for targets 1 and 2. The main reason probably is that for the selected targets the TS level for the 38 kHz transducer is lower compared to the other. Therefore, the TS locations for the 38 kHz have larger uncertainties due to the lower signal to noise ratio (Fig. 6). This causes lower signal to noise ratio (SNR) for 38 kHz which affects its performance in resolving the target position. The average TS frequency response of nine single targets are shown in Fig. 7 where targets 1–3 are the same as

4078   J. Acoust. Soc. Am. **151** (6), June 2022
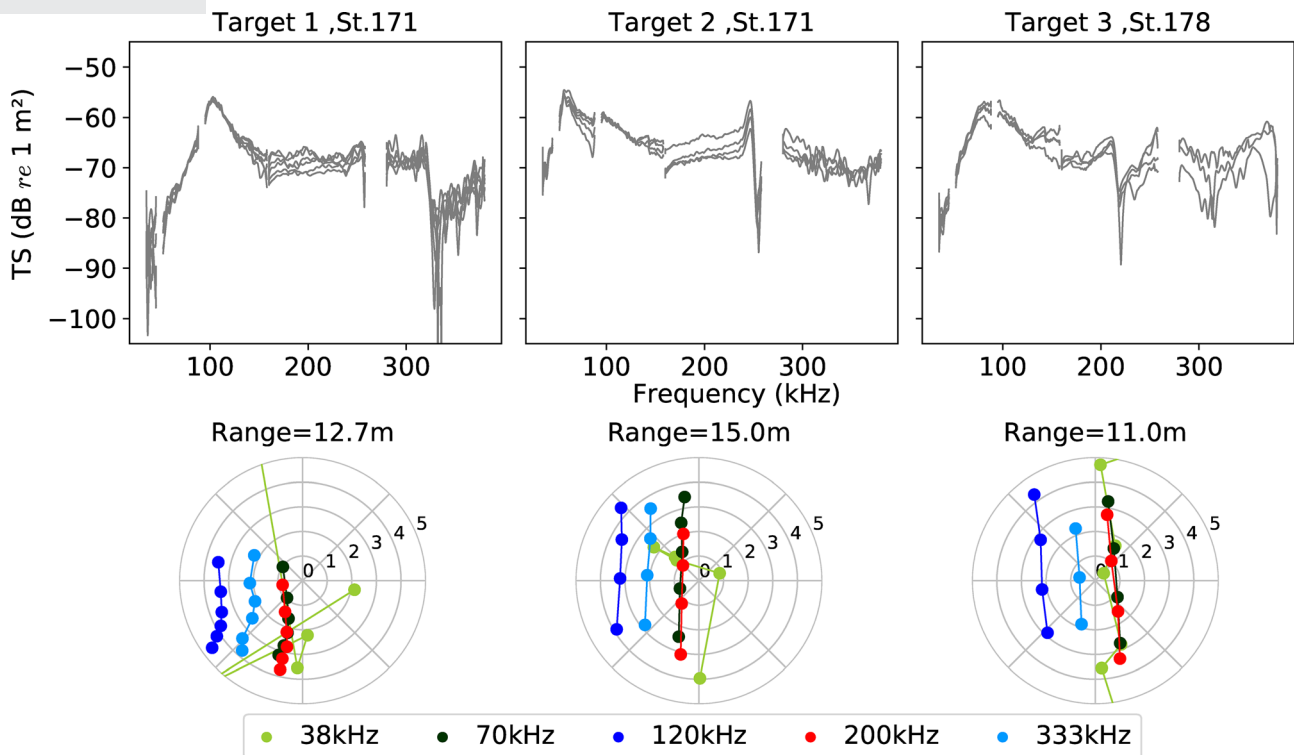
Khodabandeloo *et al.*

FIG. 6. (Color online) Top: example of *in situ* TS frequency response measurements for three single targets using broadband echosounders pinging simultaneously. The average distance of each target from the transducers is given by range. Bottom: target locations for each ping in the echosounder beams (38, 70, 120, 200, and 333 kHz). The numbers on the lower polar graphs denote the angles within the echosounder beams where "0" corresponds to the acoustic axis. For 70, 120, 200, and 333 kHz channels, the number of frequency response curves in the top graphs correspond to the number of points in the lower graphs.
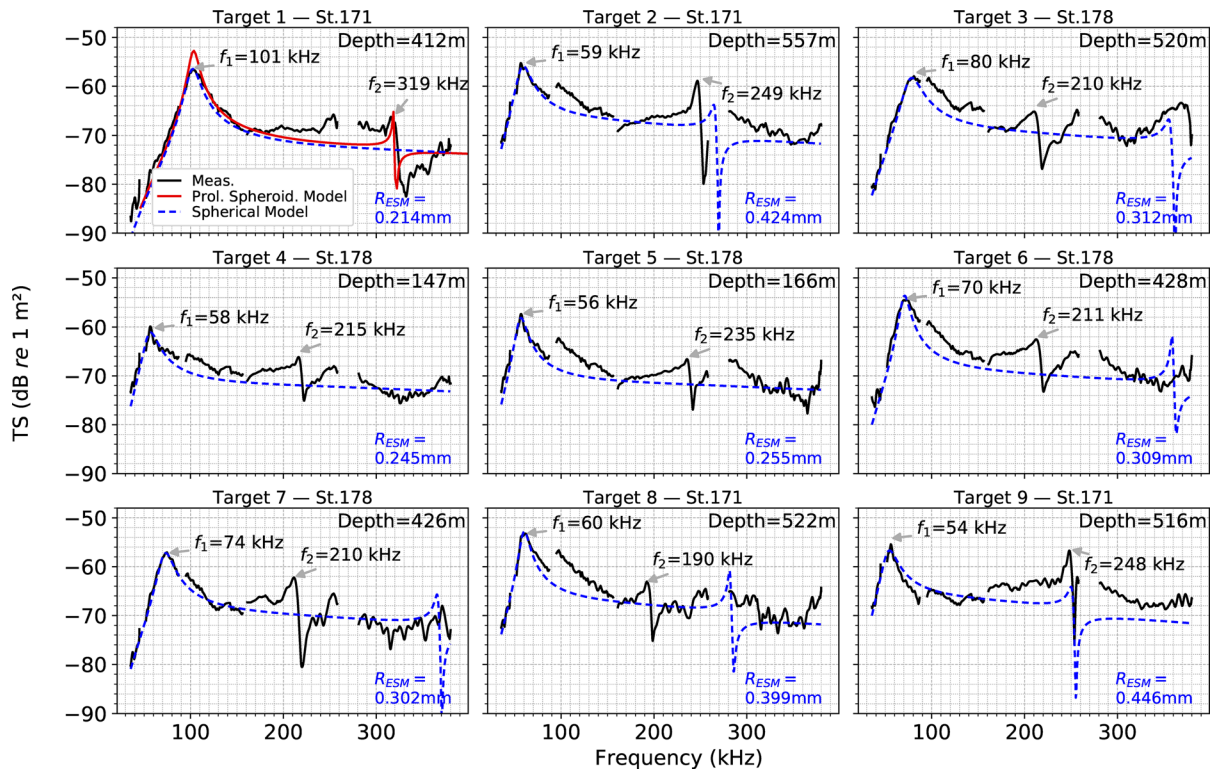

FIG. 7. (Color online) Measured wideband *in situ* TS frequency response of nine individual gas-bearing mesopelagic organisms, and their detected first and second resonance frequencies. The depth of each target is given. The viscous elastic spherical model [see Khodabandeloo *et al.* (2021b)] was used to model the spherical model TS (dashed blue line) and equivalent spherical radius estimated by the spherical model (R_{ESM}) is shown in each subplot. The prolate spheroid model shown in the first panel has $R_{ES} = 0.218$ mm and elongation of $\alpha = 2.5$ at 419 m (the closest simulation results to 412 m, see Fig. 13).

J. Acoust. Soc. Am. **151** (6), June 2022

Khodabandeloo *et al.*   4079

TABLE III. Estimated elongation for the measured targets shown in Fig. 7. $(\alpha + \beta)/2$ is the average elongation.

Target	Station No.	f_2/f_1	Depth (m)	R_{ESM} (mm)	$(\alpha + \beta)/2$ (from Fig. 3)	R_{ES} (mm) (see Fig. 8)
1	171	∼3.1	412	∼0.214	∼2.43	∼0.221
2	171	∼4.2	557	∼0.424	∼1.16	∼0.424
3	178	∼2.6	520	∼0.312	∼2.93	∼0.328
4	178	∼3.7	147	∼0.245	∼3.68	∼0.264
5	178	∼4.2	166	∼0.255	∼2.9	∼0.268
6	178	∼3	428	∼0.309	∼2.57	∼0.321
7	178	∼2.8	426	∼0.302	∼2.80	∼0.316
8	171	∼3.2	521	∼0.399	∼2.06	∼0.408
9	171	∼4.6	516	∼0.446	∼1.06	∼0.446

those shown in Fig. 6. Elongation of the nine single targets are estimated (see Table III) based on f_2/f_1 and depth using the lookup table presented in Fig. 3. By fitting TS from a viscous-elastic spherical model (Khodabandeloo *et al.*, 2021b) to the measured TS around the main resonance peak, radius of spherical gas-bubble (shown by R_{ESM}) was obtained. R_{ESM} is the equivalent spherical radius estimated by the spherical model. For the non-spherical gas-bladders, R_{ESM} underestimates the correct equivalent spherical radius, R_{ES}. Knowing the elongation, it is possible to quantify the underestimation and therefore obtain the correct value (Fig. 8). As observed in Figs. 6 and 7, there are gaps in the measured TS frequency responses between the different channels. This gap can be explained by the frequency band settings of each transducer (Table I). In addition, the quality of beginning and end of the frequency bands might be unsatisfactory and be excluded in the post-processing. If the resonance peak frequency is located within these gaps, the peak cannot be
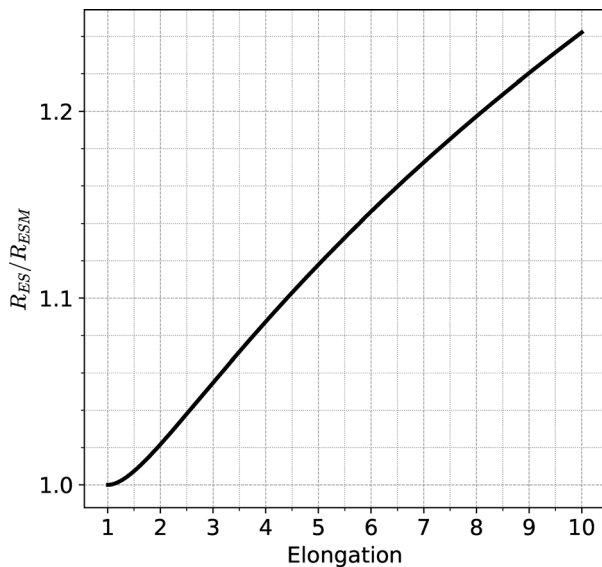
identified and, in some cases, the second peak might be misidentified. This will be further elaborated in Sec. IV. The accuracy of locating the resonance peaks depends on the frequency resolution of measured TS and quality of the data acquisition. Here, the frequency resolution is approximately 0.5 kHz. The uncertainty in locating the first or second resonance frequencies has a higher impact on the elongation estimates of more elongated gas-bladders (i.e., larger values of α) located at deeper depths (see Fig. 3).

Information about the elongation of a gas-bladder enables us to more precisely estimate its volume derived from resonance TS measurements, thereby enabling correction of estimates of equivalent spherical radius (ESR) obtained through use of spherical backscattering models (Anderson, 1950; Feuillade and Nero, 1998; Khodabandeloo *et al.*, 2021b; Love, 1978). It is known that an elongated gas bubble has higher main resonance frequency compared to the spherical gas bubble of the same volume (Ye, 1997). Following Eqs. (6)–(8) in Khodabandeloo *et al.* (2021a), a correction of the estimated ESR as a function of elongation can be obtained (Fig. 8). For example, 5% and 20% change in the ESR implies ∼16% and 73% change in the volume of the swimbladder, respectively. Therefore, the elongation factor has important implications for the buoyancy of the organisms.

The elongation of gas-bladders of a few targets from two stations (171 and 178), which were close in latitude, but with around 28° difference in longitudes, are compared in Fig. 9. The deep scattering layers (DSLs) at these two stations differed in appearance on the echograms, with the DSL(s) occupying a much larger vertical range at station 171. For station 171, the deep scattering layer is located between 300 and 700 m with two more dense layers around 350 and 600 m. On the other hand, for station 178 the deep scattering layer is more concentrated around 400 m, with very little backscatter originating from deeper than 500 m. From the TS frequency response of selected single targets, the first and second resonance frequencies were located, and their depth information were also extracted from the MESSOR's log files and their range within the transducers beam. Subsequently, the estimated elongations and their distribution from the two stations are plotted (Fig. 9). For the selected targets, the average elongation of gas-bladders for station 171 and 178 are 1.49 ± 0.52 and 2.86 ± 0.50, respectively.

IV. DISCUSSION AND CONCLUSIONS

Among the organisms in the deep scattering layers, gas-bearing ones are strong acoustic scatterers at the frequencies (∼18–450 kHz) commonly used in fishery acoustics. This makes them a critical component in the analysis of collected acoustic data, and knowledge of their acoustic properties is necessary for converting acoustic measurements to estimates of biomass. Improved knowledge about the volume and elongation of swimbladders of mesopelagic fishes has been identified as a crucial factor to reduce the overall

FIG. 8. Correct equivalent spherical radius (R_{ES}) of gas-bladder from the under-estimated spherical radius estimated by a spherical model (R_{ESM}) as a function of elongation (i.e., major to minor axis). R_{ESM} can be estimated by fitting modeled TS from a spherical backscattering model to the measured TS around the main resonance frequency.
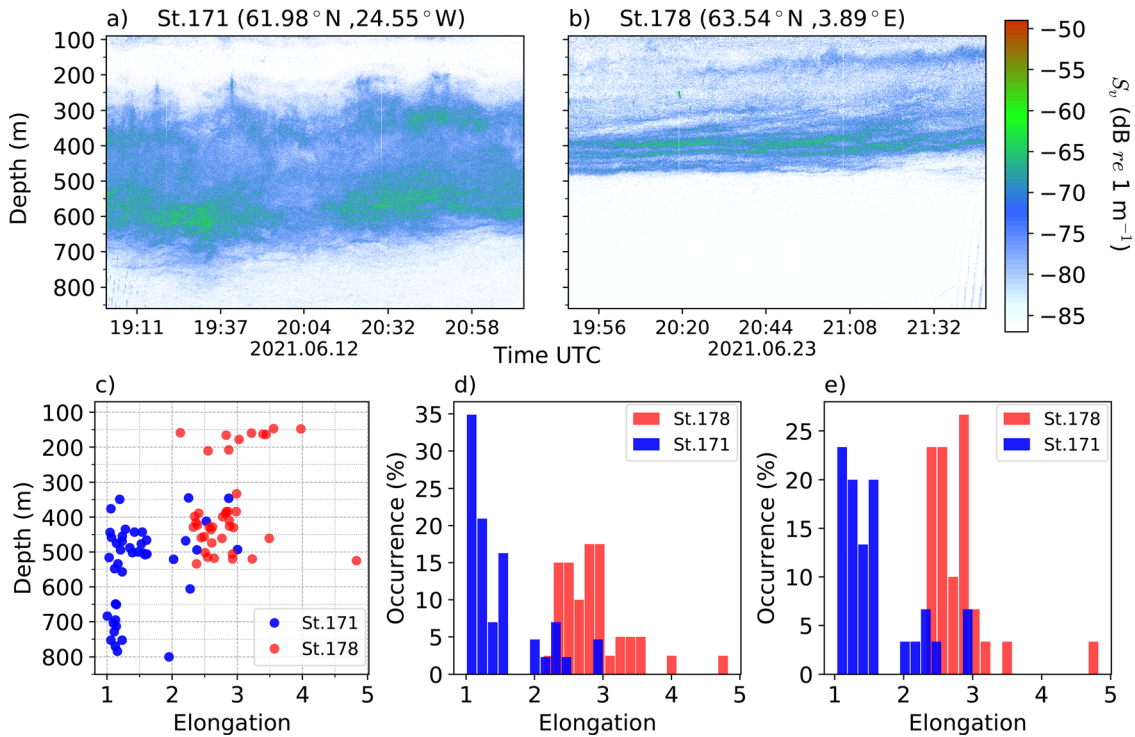
FIG. 9. (Color online) Echograms for 70 kHz from the area of two stations (a) 171 and (b) 178. (c) The estimated elongation of gas bladder from TS frequency response of 43 single targets selected from station 171 and 40 targets from station 178 are shown as a function of depth. (d) Elongation distribution of all targets from both stations. (e) The elongation distribution of the targets between 300 and 600 m.

uncertainties in acoustic based estimates of mesopelagic biomass (Proud *et al.*, 2019).

In this paper, a method was suggested to estimate the elongation of a gas-bladder from measured wideband TS frequency responses by locating the first and second resonance frequencies. Effects of elongation, orientation, and gas density on the TS frequency response, and specifically first and second resonance frequencies, were studied using a prolate spheroid model (Fig. 2). Orientation (i.e., incident angle) does not affect the locations of resonance frequencies, but influences their peak amplitude. This is shown for the modeled TS frequency responses of a prolate spheroid and egg-shaped bubble for different incident angles (Fig. 10). Increasing the incident angle from 30° to 90°, the amplitude of the second resonance frequency decreases while it increases for the third resonance frequency. For prolate spheroid, the second resonance peak vanishes at broadside incidence ($\phi = 90°$). Prolate spheroid, unlike egg-shaped object, is symmetric and therefore its TS for the incident angles 75° and 105° are the same. On the other hand, the resonance frequency locations vary with elongation and depth, and at a given depth the ratio of second to the first peak frequency (f_2/f_1) can characterize the elongation (Fig. 3). It was assumed that the physoclist swimbladder of mesopelagic fish is mainly filled with oxygen (Berg and Steen, 1968; Ross, 1976; Wittenberg *et al.*, 1980). For different gas content, such as the carbon monoxide of siphonophores (Mackie *et al.*, 1988; Pickwell *et al.*, 1964), Figure 3 needs to be modified. Furthermore, using the ratio of frequencies makes the results independent of size, as the size is defined

relative to the wavelength. In other words, the frequency axis is stretched or compressed for a larger or smaller target, respectively (see Fig. 11). The slight difference ($<0.4\%$) between f_2/f_1 of different sizes is caused by the inaccuracy of locating f_1 and f_2 due to the modeling frequency resolution (0.25 kHz). The effects of deviation from a prolate spheroid shape on the first and second peak frequencies were investigated (Sec. III C) by comparing an egg-shaped object and an ellipsoid. For the egg-shape, which is an object axisymmetric about its major axis, the locations of peak frequencies were almost the same as a prolate spheroid with the same elongation and volume. For the ellipsoid cases, it was observed that the locations of the peak frequencies are independent of orientation, same as for the prolate spheroid case. Furthermore, f_2/f_1 for an ellipsoid with elongations defined by α and β is very similar to that of a prolate spheroid with an elongation of $(\alpha + \beta)/2$. For example, as observed in Fig. 5 and Table II, f_2/f_1 the cases C6 and C7 only show a ~2% difference compared to C2.

The correct elongation estimation by the suggested method relies on the accurate identifications of f_1 and f_2, the first and second resonance frequencies, respectively. The backscattering around the first resonance frequency is very distinct and it can be plainly determined whether it is within the measured frequencies. For the targets shown in Fig. 12, f_1 is present for target 10 at ~59 kHz, while it is located below the measured frequencies for targets 11 and 12. The identification of the second resonance frequency is more challenging as it might be located below the measured frequencies, within the gap bands, or be absent due to the angle

J. Acoust. Soc. Am. **151** (6), June 2022
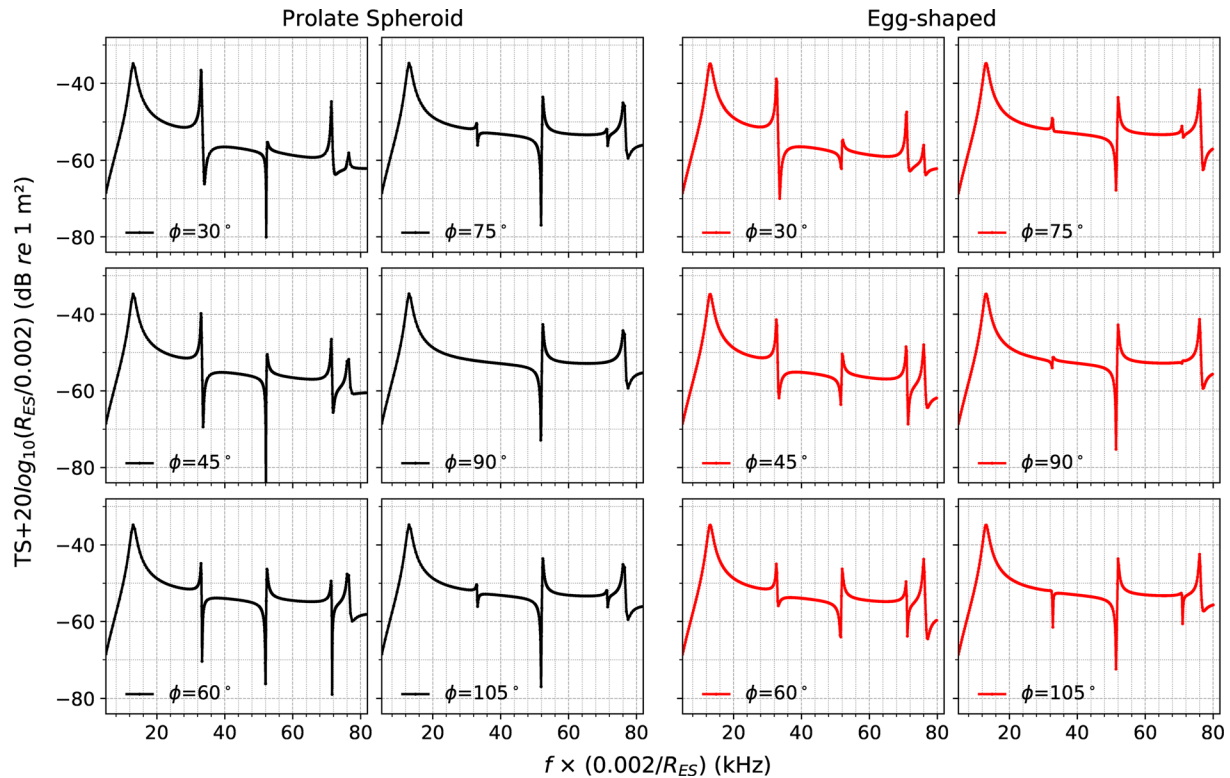
Khodabandeloo *et al.*   4081

FIG. 10. (Color online) Target strength frequency response of oxygen filled prolate spheroid (1st and 2nd columns) and egg-shape (3rd and 4th columns) with $R_{ES} = 2$ mm and elongation $\alpha = 3$, for different incident angles $\phi = 30°, 45°, 60°, 75°, 90°$, and $105°$. Due to symmetry of prolate spheroid, its TS for incident angles $75°$ and $105°$ are the same.

of incident (e.g., $\phi = 90°$ for prolate spheroid as observed in Fig. 10). However, the modeling results (Fig. 10) indicate some differences between the characteristics of the second and third resonances which probably can be used to avoid their misidentification. For example, in all cases the third resonance peak appears after a null. On the other hand, for most of the cases except the broadside for egg-shape, the second peak precede the null. Accordingly, for the examples shown in Fig. 12, the second peak is not identifiable for target 10 while for target 11 it is most likely the one at ~185 kHz. For target 12, the peak at ~140 kHz succeeds a null and probably is not the second resonance frequency.

An alternative approach to estimate the gas-bladder shape (or elongation) is to use extractive methods such as x rays. For some mesopelagic species gas-bladder shapes of dead organisms have been mapped by, for example, x rays (Fujino *et al.*, 2009; Sobradillo *et al.*, 2019; Yasuma *et al.*, 2010). However, bringing up mesopelagic organisms from deep layers to the surface is challenging, and it is uncertain if the swimbladder's morphology and volume is the same at the surface as in deep water (Sobradillo *et al.*, 2019). Therefore, the opportunity to obtain information on gas-bladder morphology of mesopelagic species using non-extractive methods such as *in situ* wideband backscattering measurements may avert other methodology problems.

The method was applied to estimate the elongation of the gas-bladder of mesopelagic organisms from *in situ* wideband acoustic measurements. From the measured
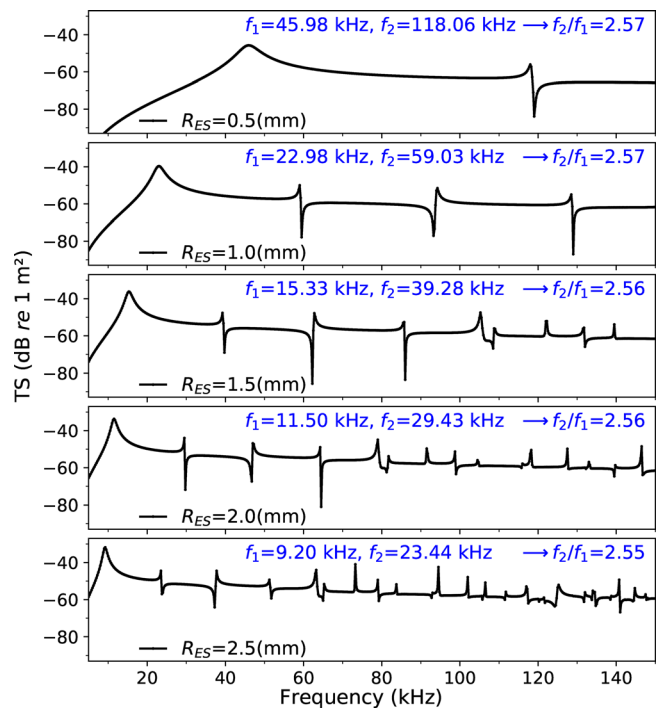
FIG. 11. (Color online) Modeled TS frequency response of prolate spheroids of different sizes $R_{ES} = 0.5, 1, 1.5, 2$, and 2.5 (mm) but with the same elongation of 3.5 and gas density of 60 kg m^{-3}. The incident angle was $60°$. The frequency spacing (resolution) for modeling TS values was 0.25 kHz. The location of the first (f_1) and second (f_2) resonance frequencies are estimated by interpolating (spline interpolation function) between the values around the corresponding peaks.

4082   J. Acoust. Soc. Am. **151** (6), June 2022

Khodabandeloo *et al.*

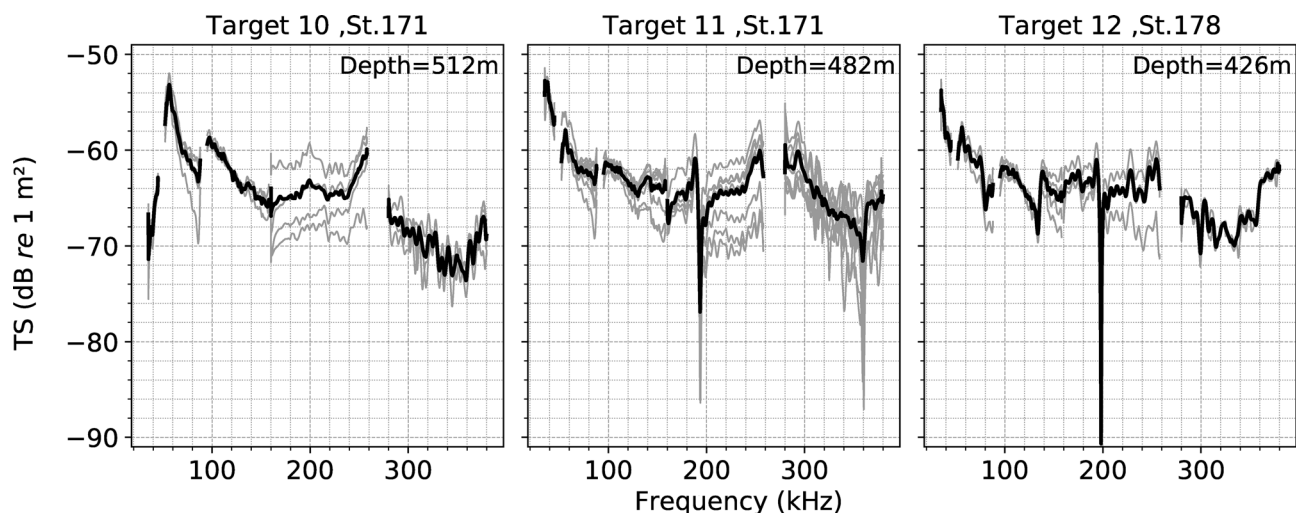FIG. 12. Example of the *in situ* measured TS where either the first or second resonance frequencies are unidentifiable. Gray lines show the TS for each ping and the thick black line is the averaged TS. For target 10, only the first resonance frequency is identifiable (∼58 kHz). The first resonance frequencies of both targets 11 and 12 are below the measured frequency range. The second resonance frequency of target 11 seems to be around 190 kHz while it is more uncertain for target 12. Especially since the observed peak at around 140 kHz has a null before itself.

backscattering of single organisms (e.g., Fig. 6), f_1 and f_2 were identified from their mean TS frequency response (Fig. 7) and the ratio f_2/f_1 was obtained. Having f_2/f_1 and depth information, the gas-bladders' elongations were estimated using Fig. 3 and summarized in Table III.

The results obtained from the two stations shows clear indication of clustering per station, i.e., average elongation differs between the two stations. This is likely due to the different taxonomic and size compositions of the targets in the two areas, as assessed through trawl catches [Institute of Marine Research, unpublished data, see also Klevjer *et al.* (2020)]. However, these differences in elongations underline the challenges to large scale modelling of target strengths of mesopelagic species, as acoustic properties are dependent on taxonomic composition, shape, and size distributions. *A priori* choice of parameter values is challenging, and a single "best estimate" value is unlikely to be sufficient to cover the natural variability. We observe little vertical variation in the elongation of gas-bladders inside stations, which is perhaps surprising, as a vertical zonation of organism is a common assumption in pelagic ecology, with species usually assumed to be occupying distinct vertical strata. Future studies should aim to assess the applicability of using the elongation factor, perhaps in combination with other acoustic properties, as an indicator of taxonomy.

Acoustic categorization is often used to attempt to separate backscattering into different taxonomic categories. In this regard, one approach is to categorize based on the aggregate—or multiple target—backscattering measurements (Horne, 2000, 2000; Jech and Michaels, 2006; Korneliussen *et al.*, 2016; Korneliussen and Ona, 2002). The other approach looks into the backscattering of individuals and allows for sorting based upon the TS frequency responses (Agersted *et al.*, 2021b; Bassett *et al.*, 2020). A recent, novel approach used acoustic models to train automatic classifiers (Cotter *et al.*, 2021), but that method still relies on good

parameter input (e.g., damping factor, elongation, and material properties) to the scattering models. Since swimbladder elongation is a morphological attribute, it may be useful in linking acoustic and taxonomic categories, especially in combination with other derived estimates of physiology, such as swimbladder size, flesh density (Agersted *et al.*, 2021a), or viscosity (Khodabandeloo *et al.*, 2021a). For instance, the swimbladders of Stomiatoid and Myctophids are reportedly very distinct (Marshall, 1960, Table I, p. 54), and deep-sea fishes with fat-invested swimbladder in their adult life stage, such as species of Cyclothone, must have a gas-filled swimbladder during the early stages of their life (Marshall, 1960). Acoustic estimates of swimbladder morphology may therefore have a high potential for taxonomic identification. One avenue of future research would be to study whether the elongation factor can be used to directly identify gas-bearing siphonophores, since backscatter from siphonophores is a potential bias in global estimates of mesopelagic fish biomass (Proud *et al.*, 2019). While our data collection and methods are geared specifically towards mesopelagic fish, our method should be general, and may later be focused on other groups, larger fish or fish larvae, both with a careful choice of frequency range employed.
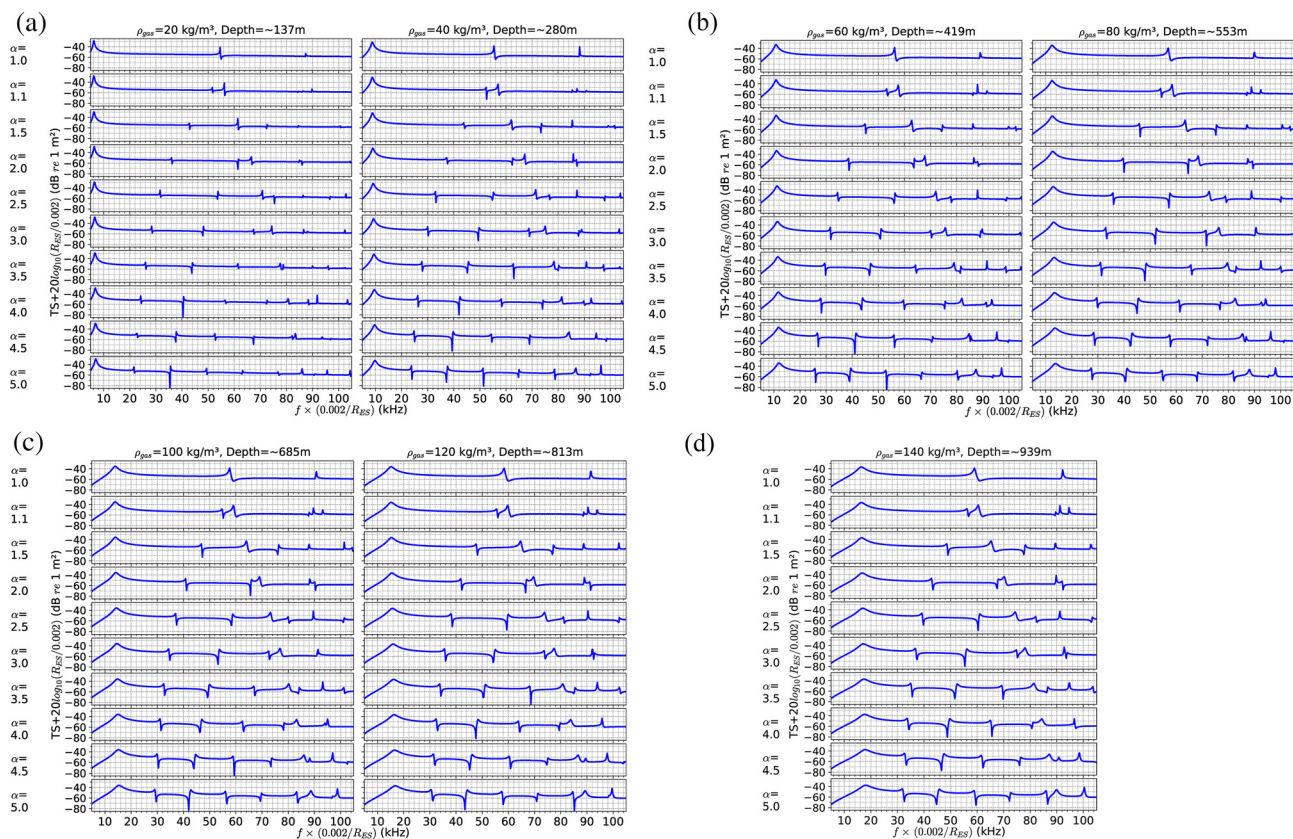
ACKNOWLEDGMENTS

FIG. 13. (Color online) Target strength frequency response of oxygen filled prolate spheroid with 2 mm equivalent spherical radius at different depths (i.e., different gas density ρ_{gas}) with different elongations (α). The TS frequency responses can be scaled for different equivalent spherical radius, R_{es}. The TS frequency responses are modeled for incident angle of $60°$. In the first set of graphs ($\rho = 20 \, \text{kg m}^{-3}$), the first and second resonance peaks occur at ~ 7 and 22 kHz, respectively.

APPENDIX

Target strengths as a function of frequency for an oxygen filled prolate spheroid of different elongation at different depths for the incident angle of $60°$ are shown in Fig. 13.

Agersted, M. D., Khodabandeloo, B., Klevjer, T. A., García-Seoane, E., Strand, E., Underwood, M. J., and Melle, W. (**2021a**). "Mass estimates of individual gas-bearing mesopelagic fish from *in situ* wideband acoustic measurements ground-truthed by biological net sampling," ICES J. Mar. Sci. **78**, 3658–3673.

Agersted, M. D., Khodabandeloo, B., Liu, Y., Melle, W., and Klevjer, T. A. (**2021b**). "Application of an unsupervised clustering algorithm on *in situ* broadband acoustic data to identify different mesopelagic target types," ICES J. Mar. Sci. **78**, 2907–2921.

Andersen, L. N., Ona, E., and Macaulay, G. J. (**2013**). "Measuring fish and zooplankton with a broadband split beam echo sounder," in *IEEE Oceans'13*, Bergen, Norway.

Anderson, V. C. (**1950**). "Sound scattering from a fluid sphere," J. Acoust. Soc. Am. **22**, 426–431.

Au, W. W. L., and Benoit-Bird, K. J. (**2003**). "Acoustic backscattering by Hawaiian lutjanid snappers. II. Broadband temporal and spectral structure," J. Acoust. Soc. Am. **114**, 2767–2774.

Barham, E. G. (**1963**). "Siphonophores and the deep scattering layer," Science **140**, 826–828.

Bassett, C., Lavery, A. C., Stanton, T. K., and Cotter, E. D. (**2020**). "Frequency- and depth-dependent target strength measurements of individual mesopelagic scatterers," J. Acoust. Soc. Am. **148**, EL153–EL158.

Berenger, J. P. (**1994**). "A perfectly matched layer for the absorption of electromagnetic waves," J. Comput. Phys. **114**, 185–200.

Berg, T., and Steen, J. B. (**1968**). "The mechanism of oxygen concentration in the swim-bladder of the eel," J. Physiol. **195**, 631–638.

Cakoni, F., and Colton, D. (**2005**). *Qualitative Methods in Inverse Scattering Theory: An Introduction* (Springer Science & Business Media, New York).

Chu, D. (**2011**). "Technology evolution and advances in fisheries acoustics," J. Mar. Sci. Technol. **19**, 245–252.

Clay, C. S., and Horne, J. K. (**1994**). "Acoustic models of fish: The Atlantic cod (*Gadus morhua*)," J. Acoust. Soc. Am. **96**, 1661–1668.

COMSOL Multiphysics (**2020**). *COMSOL Multiphysics 5.6 Acoustics Module User Guide* (COMSOL, Inc., Burlington, MA).

Cotter, E., Bassett, C., and Lavery, A. (**2021**). "Classification of broadband target spectra in the mesopelagic using physics-informed machine learning," J. Acoust. Soc. Am. **149**, 3889–3901.

Feuillade, C., and Nero, R. W. (**1998**). "A viscous-elastic swimbladder model for describing enhanced-frequency resonance scattering from fish," J. Acoust. Soc. Am. **103**, 3245–3255.

Foote, K. G. (**1980**). "Importance of the swimbladder in acoustic scattering by fish: A comparison of gadoid and mackerel target strengths," J. Acoust. Soc. Am. **67**, 2084–2089.

Fujino, T., Sadayasu, K., Abe, K., Kidokoro, H., Tian, Y., Yasuma, H., and Miyashita, K. (**2009**). "Swimbladder morphology and target strength of a mesopelagic fish, *Maurolicus japonicus*," J. Mar. Acoust. Soc. Jpn. **36**, 241–249.

Gjoesaeter, J., and Kawaguchi, K. (**1980**). "A review of the world resources of mesopelagic fish," FAO Fisheries Technical Papers (FAO), https://agris.fao.org/agris-search/search.do?recordID=XF8003729 (Last viewed 1/10/2021).

Godø, O. R., Handegard, N. O., Browman, H. I., Macaulay, G. J., Kaartvedt, S., Giske, J., Ona, E., Huse, G., and Johnsen, E. (**2014**). "Marine ecosystem acoustics (MEA): Quantifying processes in the sea at the spatio-temporal scales on which they occur," ICES J. Mar. Sci. **71**, 2357–2369.

Grimaldo, E., Grimsmo, L., Alvarez, P., Herrmann, B., Møen Tveit, G., Tiller, R., Slizyte, R., Aldanondo, N., Guldberg, T., Toldnes, B., Carvajal, A., Schei, M., and Selnes, M. (**2020**). "Investigating the potential for a commercial fishery in the Northeast Atlantic utilizing mesopelagic species," ICES J. Mar. Sci. **77**, 2541–2556.

Harari, I. (**2006**). "A survey of finite element methods for time-harmonic acoustics," Comput. Methods Appl. Mech. Eng. **195**, 1594–1607.

Haslett, R. W. G. (**1965**). "Acoustic backscattering cross sections of fish at three frequencies and their representation on a universal graph," Br. J. Appl. Phys. **16**, 1143–1150.

Horne, J. K. (**2000**). "Acoustic approaches to remote species identification: A review," Fisheries Oceanogr. **9**, 356–371.

Ihlenburg, F. (**1998**). *Finite Element Analysis of Acoustic Scattering, Applied Mathematical Sciences* (Springer-Verlag, New York), Vol. 132.

Irigoien, X., Klevjer, T. A., Røstad, A., Martinez, U., Boyra, G., Acuña, J. L., Bode, A., Echevarria, F., Gonzalez-Gordillo, J. I., Hernandez-Leon, S., Agusti, S., Aksnes, D. L., Duarte, C. M., and Kaartvedt, S. (**2014**). "Large mesopelagic fishes biomass and trophic efficiency in the open ocean," Nat. Commun. **5**, 3271.

Jech, M. J., and Michaels, W. L. (**2006**). "A multifrequency method to classify and evaluate fisheries acoustics data," Can. J. Fish. Aquat. Sci. **63**, 2225–2235.

Kaartvedt, S., Røstad, A., Klevjer, T. A., and Staby, A. (**2009**). "Use of bottom-mounted echo sounders in exploring behavior of mesopelagic fishes," Mar. Ecol. Prog. Ser. **395**, 109–118.

Kechroud, R., Soulaimani, A., Saad, Y., and Gowda, S. (**2004**). "Preconditioning techniques for the solution of the Helmholtz equation by the finite element method," Math. Comput. Simul. **65**, 303–321.

Khodabandeloo, B., Agersted, M. D., Klevjer, T., Macaulay, G. J., and Melle, W. (**2021b**). "Estimating target strength and physical characteristics of gas-bearing mesopelagic fish from wideband *in situ* echoes using a viscous-elastic scattering model," J. Acoust. Soc. Am. **149**, 673–691.

Khodabandeloo, B., Agersted, M. D., Klevjer, T. A., Pedersen, G., and Melle, W. (**2021a**). "Mesopelagic flesh shear viscosity estimation from *in situ* broadband backscattering measurements by a viscous–elastic model inversion," ICES J. Mar. Sci. **78**, 3147–3161.

Khodabandeloo, B., Ona, E., Macaulay, G. J., and Korneliussen, R. (**2021c**). "Nonlinear crosstalk in broadband multi-channel echosounders," J. Acoust. Soc. Am. **149**, 87–101.

Klevjer, T. A., Irigoien, X., Røstad, A., Fraile-Nuez, E., Benítez-Barrios, V. M., and Kaartvedt, S. (**2016**). "Large scale patterns in vertical distribution and behaviour of mesopelagic scattering layers," Sci. Rep. **6**(1), 19873.

Klevjer, T. A., Melle, W., Knutsen, T., and Aksnes, D. L. (**2020**). "Vertical distribution and migration of mesopelagic scatterers in four north Atlantic basins," Deep Sea Res. Part II **180**, 104811.

Knutsen, T., Melle, W., Mjanger, M., Strand, E., Fuglestad, A.-L., Broms, C., Bagøien, E., Fitje, H., Ørjansen, O., and Vedeler, T. (**2013**). "MESSOR—A towed underwater vehicle for quantifying and describing the distribution of pelagic organisms and their physical environment," in *2013 MTS/IEEE OCEANS–Bergen*, pp. 1–12.

Korneliussen, R. J., Heggelund, Y., Macaulay, G. J., Patel, D., Johnsen, E., and Eliassen, I. K. (**2016**). "Acoustic identification of marine species using a feature library," Meth. Oceanogr. **17**, 187–205.

Korneliussen, R. J., and Ona, E. (**2002**). "An operational system for processing and visualizing multi-frequency acoustic data," ICES J. Mar. Sci. **59**, 293–313.

Love, R. H. (**1971**). "Measurements of fish target strength: A review," Fish. B-NOAA **69**, 703–715.

Love, R. H. (**1978**). "Resonant acoustic scattering by swimbladder-bearing fish," J. Acoust. Soc. Am. **64**, 571–580.

Mackie, G. O., Pugh, P. R., and Purcell, J. E. (**1988**). "Siphonophore biology," in *Advances in Marine Biology* (Elsevier, Amsterdam), Vol. 24, pp. 97–262.

MacLennan, D. N. (**1981**). "The theory of solid spheres as sonar calibration targets," Scottish Fisheries Research Report Number 22, Department of Agriculture Fisheries, Marine Laboratory, Aberdeen, Scotland.

Marshall, N. B. (**1951**). "Bathypelagic fishes as sound scatterers in the ocean," J. Marine Res. **10**, 1–17.

Marshall, N. B. (**1960**). *Swimbladder Structure of Deep-Sea Fishes in Relation to Their Systematics and Biology* (Cambridge University Press, Cambridge), Vol. 27, pp. 1–121.

Naik, A. S., Whitaker, R. D., Albrektsen, S., Solstad, R. G., Thoresen, L., and Hayes, M. (**2021**). "Mesopelagic fish protein hydrolysates and extracts: A source of novel anti-hypertensive and anti-diabetic peptides," Front. Mar. Sci. **8**, 1169.

Olsen, R. E., Strand, E., Melle, W., Nørstebø, J. T., Lall, S. P., Ringø, E., Tocher, D. R., and Sprague, M. (**2020**). "Can mesopelagic mixed layers be used as feed sources for salmon aquaculture?," Deep Sea Res. Part II: Topical Stud. Oceanography **180**, 104722.

Ona, E. (**1990**). "Physiological factors causing natural variations in acoustic target strength of fish," J. Mar. Biol. Assoc. United Kingdom **70**, 107–127.

Ottosen, N. S., and Petersson, H. (**1992**). *Introduction to the Finite Element Method* (Prentice Hall, Englewood Cliffs, NJ).

Pickwell, G. V., Barham, E. G., and Wilton, J. W. (**1964**). "Carbon monoxide production by a bathypelagic siphonophore," Science **144**(3620), 860–862.

Proud, R., Handegard, N. O., Kloser, R. J., Cox, M. J., and Brierley, A. S. (**2019**). "From siphonophores to deep scattering layers: Uncertainty ranges for the estimation of global mesopelagic fish biomass," ICES J. Mar. Sci. **76**, 718–733.

Rao, S. S. (**2011**). *The Finite Element Method in Engineering*, 5th ed. (Butterworth-Heinemann, Burlington, VT).

Reeder, D. B., Jech, J. M., and Stanton, T. K. (**2004**). "Broadband acoustic backscatter and high-resolution morphology of fish: Measurement and modeling," J. Acoust. Soc. Am. **116**, 747–761.

Ross, L. G. (**1976**). "The permeability to oxygen of the swimbladder of the mesopelagic fish *Ceratoscopelus maderensis*," Mar. Biol. **37**, 83–87.

Simrad (**2020**). *Simrad EK80, Wide Band Scientific Echo Sounder*, reference manual.

Sobradillo, B., Boyra, G., Martinez, U., Carrera, P., Peña, M., and Irigoien, X. (**2019**). "Target strength and swimbladder morphology of Mueller's pearlside (*Maurolicus muelleri*)," Sci. Rep. **9**, 17311.

Stanton, T. K., Reeder, D. B., and Jech, J. M. (**2003**). "Inferring fish orientation from broadband-acoustic echoes," ICES J. Mar. Sci. **60**, 524–531.

Thompson, L. L. (**2006**). "A review of finite-element methods for time-harmonic acoustics," J. Acoust. Soc. Am. **119**, 1315–1330.

Vinogradov, M. E. (**1962**). "Feeding of the deep-sea zooplankton," Rapp. Rv. Réun. Cons. Perm. Int. Explor. Mer. **153**, 114–120.

Wittenberg, J. B., Copeland, D. E., Haedrich, F. R. L., and Child, J. S. (**1980**). "The swimbladder of deep-sea fish: The swimbladder wall is a lipid-rich barrier to oxygen diffusion," J. Mar. Biol. Assoc. UK **60**, 263–276.

Yasuma, H., Sawada, K., Ohshima, T., Miyashita, K., and Aoki, I. (**2003**). "Target strength of mesopelagic lanternfishes (family Myctophidae) based on swimbladder morphology," ICES J. Mar. Sci. **60**, 584–591.

Yasuma, H., Sawada, K., Takao, Y., Miyashita, K., and Aoki, I. (**2010**). "Swimbladder condition and target strength of myctophid fish in the temperate zone of the Northwest Pacific," ICES J. Mar. Sci. **67**, 135–144.

Ye, Z. (**1997**). "Low-frequency acoustic scattering by gas-filled prolate spheroids in liquids," J. Acoust. Soc. Am. **101**, 1945–1952.

Zakharia, M. (**1996**). "Wideband sounder for fish species identification at sea," ICES J. Mar. Sci. **53**, 203–208.